LASER & PHOTONICS REVIEWS
www.lpr-journal.org

Heralded Entanglement Distribution Between Two Spin-Wave Memories Using Temporally Multiplexed Scheme

Minjie Wang, Haole Jiao, Jiajin Lu, Wenxin Fan, Zhifang Yang, Mengqi Xi, Shujing Li, and Hai Wang**

The elementary link, which is formed by entanglement between two remote atomic ensembles, is a fundamental component of Duan–Lukin–Cirac–Zoller (DLCZ) quantum repeater. For practical realization of quantum repeaters, it is required that entanglement between two atomic-ensemble-based memories can be generated with high rates and retrieved with high efficiencies. However, so far, such quantum-repeater links remain challenge in experiments. Here, heralded entanglement distribution between atomic-ensemble-based memories is demonstrated via temporally multiplexed scheme. A train of 12 write pulses in time is applied to a cloud of cold atoms along different directions, which generates temporally multiplexed pairs of Stokes photons and spin waves via DLCZ processes. The Stokes fields propagating in the two spatial modes, which are paired with two spin waves are combined to perform a single-photon Bell-state measurement. A successful detection projects the two spin waves into a single-excitation entanglement, which represents entanglement distribution in an elementary link. Compared with single-mode storage scheme, the temporally multiplexed scheme gives rise to a 11.8-fold increase in entanglement generation rate. By using cavity-enhanced scheme, spin waves stored in the atoms are retrieved on demand and the retrieval efficiencies are up to 70%, which is beneficial for the subsequent entanglement swapping between adjacent links.

1. Introduction

Long-distance entanglement distribution is a fundamental task of large-scale quantum networks.[1–4] Based on quantum networks, one can implement distributed quantum computation,[5] quantum key distribution,[6] and loophole-free Bell test.[7] Long-distance entanglement distribution can be achieved by transmitting photonic information via satellite-based or fiber-based channels.[8] In future, the entanglement distribution may use a combination of the two schemes. For the fiber-based entanglement distribution, a problem is that the entanglement distribution distance is limited by the transmission losses of the optical fibers. To overcome this limitation, quantum repeater (QR) scheme[9] has been proposed. In the scheme, the distance is divided into a number of elementary links, each of which consists of two memory nodes connected by an elementary communication channel. Entanglement is first created in the single links, which corresponds to the entanglement generation between the two memories, and then it is extended over the full distance by entanglement swapping.

For practically realizing QR, Duan, Lukin, Cirac, and Zoller proposed a protocol, which combines atomic ensembles and linear optics[10] and is named DLCZ protocol. In the protocol, an elementary process is to generate non-classically correlated pairs of Stokes photons and spin waves in atomic ensembles, which corresponds to quantum interfaces.[11] Such quantum interfaces are achieved via spontaneous Raman scatterings (SRS) induced by write laser pulses. Toward the realization of the protocol, many experiments have been reported. For example, the storage lifetime of atomic spin-wave has been expanded to second order by combining magnetic-field-insensitive,[12–14] long wavelength spin-wave,[13,15] and confining the atoms in optical lattices.[16–18] The retrieval efficiency of atomic memory is improved significantly in high optical-depth cold atomic ensemble[19–21] or using the cavity-enhanced scheme.[11,15,16,22,23]

However, to achieve high quantum-correlation pairs of the Stokes photons and spin waves, the excitation probability of the pairs has to be set at a low level (about 1% per trial), which makes the long-distance communication rate incredibly low.[10,24] Multiplexing provides a solution to this problem.[25] Spatially multiplexed quantum memories have been realized by using many individually accessible memory cells with programmable

M. Wang, H. Jiao, J. Lu, W. Fan, Z. Yang, M. Xi, S. Li, H. Wang
The State Key Laboratory of Quantum Optics and Quantum Optics Devices
Institute of Opto-Electronics, Shanxi University
Taiyuan 030006, China
E-mail: lishujing@sxu.edu.cn; wanghai@sxu.edu.cn
M. Wang, H. Jiao, J. Lu, W. Fan, Z. Yang, M. Xi, S. Li, H. Wang
Collaborative Innovation Center of Extreme Optics
Shanxi University
Taiyuan 030006, China

The ORCID identification number(s) for the author(s) of this article can be found under https://doi.org/10.1002/lpor.202300825

DOI: 10.1002/lpor.202300825

addressing,[26] by spatially resolved single-photon detection[27,28] or by collecting the Stokes photon in multiple spatial directions simultaneously in cold atomic ensemble.[29,30] Temporally multiplexed DLCZ quantum interfaces that store more than 10 modes have been demonstrated with cold atomic ensembles by P. Farrera et al. (H. de Riedmatten's group[31,32]) and Y. F. Wen et al. in our group,[33,34] respectively. H. de Riedmatten's group generated the temporally multiplexed DLCZ memories by applying a train of write pulses that went through the atoms along a direction.[32] They applied a gradient magnetic field to control the dephasing and rephasing of the temporally multiplexed spin-wave memories, which enables the temporally multimode memories to be distinguishable. For controlling the dephasing and rephasing of the spin-waves, in that experiment the spin waves are stored in a magnetic-field sensitive coherence ($m = 1 \leftrightarrow m' = 1$),[32] which limits the storage lifetime.[17] In our experiment, the temporally multiplexed pairs of Stokes photons and spin waves are generated by applying a train of write pulses in time along different directions, which requires a set of acoustic-optic modulators to control the directions of the pulses. An advantage of our scheme is that the spin waves may be stored in magnetic-field insensitive coherence, which promises a longer memory lifetime. Comparing the spatial multiplexing, the temporal multiplexing is more resource efficient and scalable than spatial multiplexing due to its reuse of the same detectors.[35]

So far, one of the goals of quantum repeater is how to establish entanglement over a quantum repeater link with a high rate. Some pioneering progresses have been made in this line.[36–44] Y. Yu et al. has realized entanglement over 22 kilometers based on cavity-enhanced DLCZ memory together with efficient quantum frequency conversions. However, the entanglement generation is based on single-mode memory in that experiment,[39] which limits the entanglement generation rate. The solid-state quantum memories using atomic frequency combs scheme have a broad inhomogeneous absorption, which enables them to be used for temporal multimode operations. X. Liu et al. demonstrated the heralded entanglement between absorptive quantum memories, in which the temporal multiplexing is utilized to enhance the entanglement distribution rate.[42] D. Lago-Rivera et al. reported telecom-heralded entanglement between two temporally multimode solid-state quantum memories.[40] However, in the above two works, the memories have predetermined storage times and the efficiency is relatively low.

Here, we demonstrate heralded entanglement distribution between two memory ensembles via a temporally multiplexed scheme. A train of 12 write-laser pulses in time is applied to a cold atomic cloud along different directions, which generates temporally multiplexed pairs of Stokes photons and spin waves via DLCZ processes. The Stokes photons are collected in two spatial modes S_R and S_L, which defines two spin waves R and L (atomic collective excitations), both are temporally multiplexed memories. Since the two multiplexed spin waves can be independently stored, they are may be regarded as two memory ensembles. The two Stokes fields, which are non-classically correlated with the two memory ensembles R and L, are combined on a beam splitter for performing a single-photon Bell-state measurement (BSM). A successful detection event projects the two memories into a single-excitation entanglement, which represents the heralded entanglement distribution in a repeater link. Compared with single-mode storage scheme, the rate of entanglement generation has been increased by an order of magnitude (11.8-flod). By using the cavity-enhanced scheme, the spin waves are retrieved on demand and the retrieval efficiency is up to 70%. The demonstration of temporally multiplexed heralded entanglement distribution with on-demand and high-efficiency retrieval paves the road for practical quantum communication and quantum network.

2. Entanglement Distribution Between Two Spin-Wave Memories via a Temporally Multiplexed And Cavity-Enhanced Scheme

Our scheme for generating entanglement between two spin-wave memories via a temporally multiplexed is shown in **Figure 1**. A cold ^{87}Rb atomic cloud is used for the memories, which is placed inside a ring cavity. The retrieval efficiencies of the spin waves are enhanced by the cavity. A train of write pulses in time is applied on the atoms in different directions to create temporally multiplexed pairs of spin waves and Stokes photons via SRS processes. We collect the temporally multiplexed Stokes fields in two different spatial modes S_R and S_L. The temporally multiplexed spin waves, which are non-classically correlated with the Stokes fields in S_R (S_L) channel are denoted as R (L) memory modes. Since R (L) spin waves are stored independently, they can be regarded as two (R and L) memory ensembles.[36,45,46] The temporally multiplexed Stokes fields in S_R and S_L channels are combined on a BS to perform the single-photon BSM. When a single Stokes photon at i-th mode is detected by detector D_1 or D_2, entanglement state between two memory ensembles R and L is successfully established.

To verify the entanglement state between two memory ensembles, we apply a strong read laser pulse, which propagate along the counter-direction to the i-th write pulse, onto the atoms. Thus, the spin waves L and R that are stored in the i-th modes are mapped into anti-Stokes photons. Constrained to the phase-match condition (details see below), the retrieved anti-Stokes photons direct into the aS_R and aS_L modes that propagate along the direction with a 180^o angle to that of S_R and S_L fields, respectively. In our present experiment, the S_R and S_L fields resonate with the cavity, which enhance the interaction between light and atoms and significantly improve the retrieval efficiency.[15]

In the presented work, we demonstrate entanglement distribution between two atomic memories with an atomic ensemble via multiplexing DLCZ scheme. In real quantum repeaters, the individual quantum-repeater links are formed by two remote nodes (atomic memories). Our multiplexed memory scheme together with high-efficiency retrieval may be found applications in practical DLCZ repeater protocol to improve the repeater rate. To explain such an improvement, we calculate the rate of distributing entanglement over the quantum repeater formed by several elementary links with multiplexed and non-multiplexed schemes, respectively.

The success probability for generating entanglement in single links with nodes using N-mode multiplexing memories can be evaluated by[25]

$$P_0^{(N)} = 1 - (1 - P_0)^N \approx NP_0 \quad (1)$$

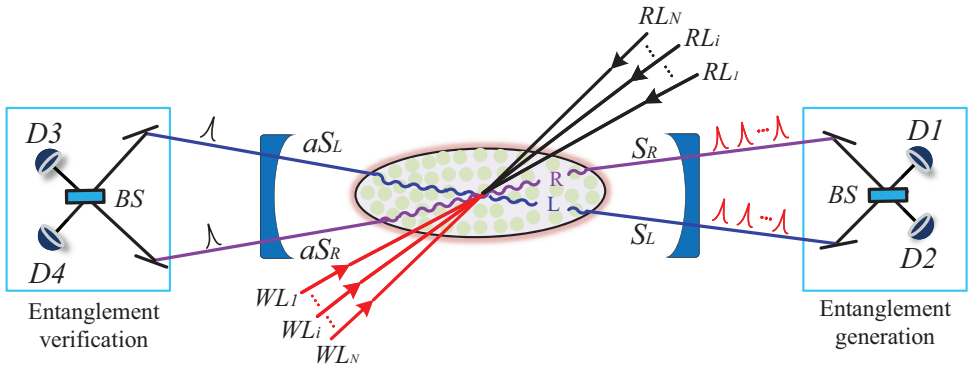

Figure 1. Schematic view of generating temporally multiplexed entanglement between two spin-wave memories. A cold atomic cloud is used as the memory medium, which is placed inside a ring cavity to enhance the retrieval efficiencies of the spin waves. A train of write laser pulses (WL_1, WL_2..... and WL_N) is applied onto atoms from different directions, to create the temporally multiplexed (*1*-st,...*i*-th... *N*-th) non-classically correlated pairs of Stokes photons and spin waves. The temporal-multiplexed Stokes fields direct into two spatial modes S_R and S_L, respectively, are collective and combined on a beam splitter (BS). The Stokes fields SR and S_L define the two spin waves *R* and *L*, respectively. The two outputs of BS are sent to detectors D_1 and D_2, respectively, for Bell state measurement (BSM). Conditioned on a coincident event between D_1 or D_2 at *i*-th time mode (with *i*=1 to *N*), the two memories *R* and *L* are projected into an entanglement state. To verify the entanglement state, we apply the read laser (*RL*) pulse propagating along the counter-direction to the *i*-th write pulse to convert the spin waves *R* and *L* which is stored in the *i*-th mode into the anti-Stokes fields aS_R and aS_L, respectively. Thus, entanglement between the two memories is transferred to that between the fields aS_R and aS_L.

where $P_0 = \chi e^{-L_0/(2L_{att})}\eta_{FC}\eta_{TD}$ is the success entanglement generation probability for the case each node store single (non-multiplexed) mode, χ is the excitation probability of each node, L_{att} is the attenuation length of the fiber channel, L_0 is the distance between two quantum memory, η_{FC} is the memory-to-telecom frequency conversion efficiency; η_{TD} is the total detection efficiency. So, the *N*-mode memory scheme gives rise to a *N*-fold increase in entanglement generation in single links, compared with non-multiplexed scheme. Only one attempt at entanglement generation can be performed per communication interval $T_{cc} = L_0/c$, where c is the speed of light in fibers. So the time required to establish entanglement in a elementary link is $t_0 \simeq T_{cc}/P_0^{(N)} = T_{cc}/(NP_0)$.

The success probability for entanglement swapping between two adjacent repeater links at the 1-st nest level is $P_1 = R_0 e^{-t_0/\tau_0}\eta_{TD}$, where τ_0 is the memory lifetime in atomic ensembles, and R_0 is the retrieval efficiency at zero delay. The success probability for entanglement swapping at the *i*-th level is $P_j = R_0 e^{-t_{i-1}/\tau_0}\eta_{TD}$, where $t_i \simeq t_{i-1}/P_i$ is the time needed for the entanglement swapping at the *i*-th level. It is assumed that *n*-level entanglement swapping is required to distribute entanglement to the whole communication channel. Then the communication rate can be expressed as:

$$R_{rate} \approx \frac{1}{T_{cc}} P_0^{(N)} \left(\prod_{i=1}^{i=n} P_i\right) P_{pr} \tag{2}$$

where $P_{pr} \approx R_0 e^{-t_n/\tau_0}$ is the success probability for distributing an entangled photon pair over the distance *L*.

We assume $n = 4$, $L_0 = 63$ km, and the distance between two remote quantum nodes is

1000 km. The total detection efficiency $\eta_{TD} \approx 90\%$ for the Stokes (anti-Stokes) detection channel. The memory lifetime $\tau_0 = 16$s[45] and quantum frequency conversion efficiency $\eta_{FC} = 46\%$[46] are the best experimental performance at present as far as we know. With the retrieval efficiency at 80% and the mode number at 100, the communication rate can reach 1Hz, which holds promise for long-distance quantum communication.

3. Experimental Demonstration of Temporally Multiplexed Entanglement Distribution

A cloud of cold ^{87}Rb atoms trapped in magneto-optical trap (MOT) is used for demonstrating DLCZ entanglement. After the atoms are released from MOT, we apply a bias magnetic field (B = 4G) along *Z* axis to define the quantization axis of the atoms. A ring-cavity is placed around the atoms to improve the retrieval efficiency of DLCZ memories, whose details can be found in our previous work.[15]

The atomic ground levels $|g\rangle = |5S_{1/2}, F=1\rangle$ and $|s\rangle = |5S_{1/2}, F=2\rangle$ together with the excited level $|e_1\rangle = |5P_{1/2}, F'=1\rangle$ ($|e_2\rangle = |5P_{1/2}, F'=2\rangle$) form a Λ -type system, shown in **Figure** 2b,c. The atoms are initially prepared in the Zeeman state $|g, m_{F_g}=0\rangle$. A train of 12 write pulses, each of which propagates along different propagation directions, is applied to the atoms to create the temporally multiplexed (*i*-th, with $i = 1$ to 12) non-classically correlated pairs of Stokes photons and spin waves via SRS. The angle between the two adjacent write pulses is 0.28°, and the angle between the 1-st write pulse and *Z* axis is 0.2°. The train lasts ΔT=8μs and the interval between two adjacent write pulses is 400ns. All write pulses are σ^+-polarized with red-detuned by 110 MHz to the $|g\rangle \rightarrow |e_1\rangle$ transition. Each write pulse induces the Raman transition $|g, m_{Fg}=0\rangle \rightarrow |s, m_{Fs}=0\rangle$ via $|e_1, m_{Fe_1}=1\rangle$, which emits a σ^+-polarized Stokes photon and simultaneously creates an atomic spin-wave associated with the clock coherence $|m_{Fg}=0\rangle \leftrightarrow |m_{Fs}=0\rangle$ probabilistically.

We collect the temporally multiplexed Stokes fields in two spatial modes (channel) S_L and S_R, where, the angles of S_L (S_R)

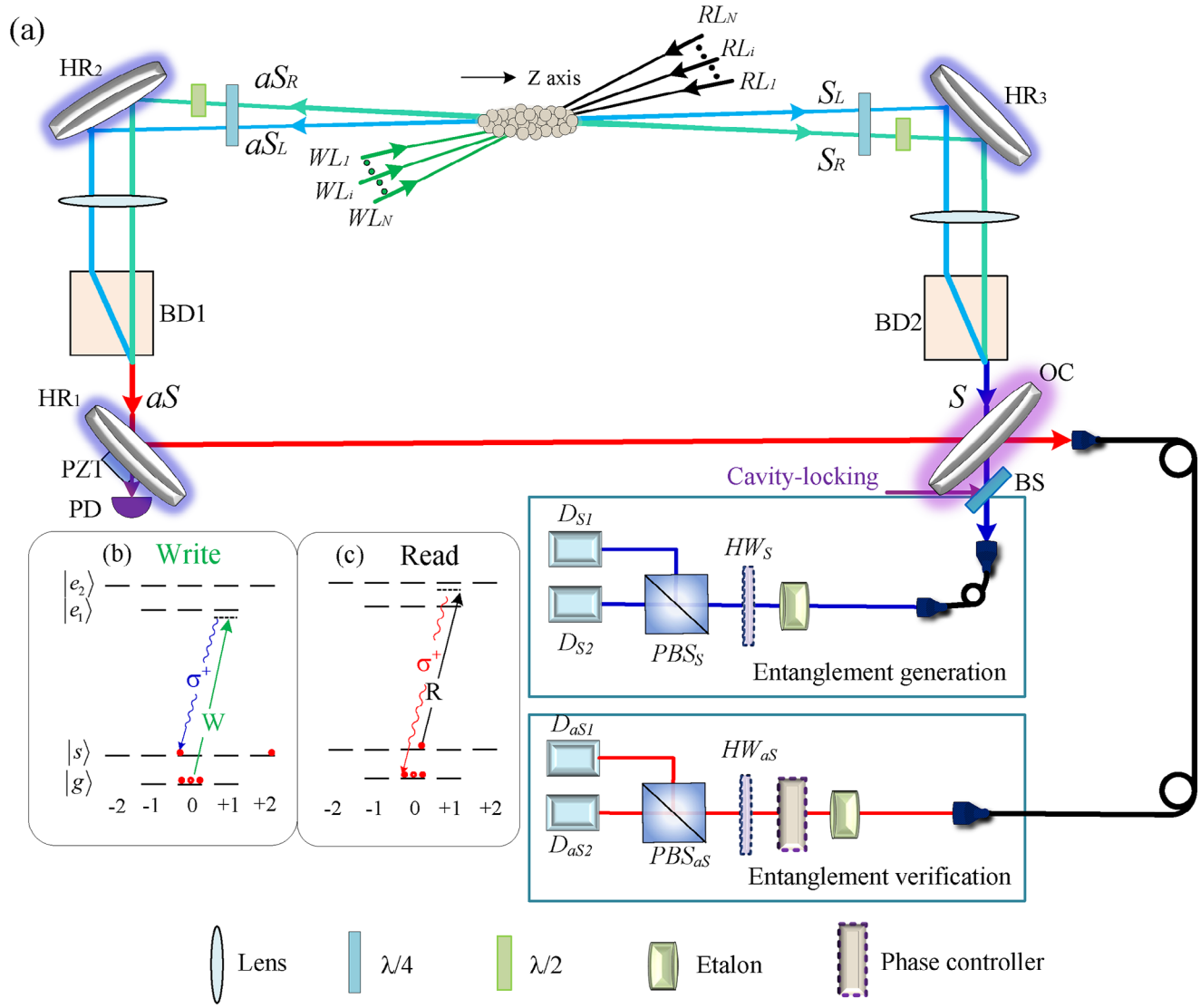

Figure 2. Schematic diagram of entanglement generation between two temporally multiplexed memory ensembles. a) Experimental setup. A train of write laser pulses (WL_1, WL_2..... and WL_N) is applied onto a cold atomic ensemble along different directions, to create the temporally-multiplexed (1-st,...*i*-th... *N*-th) non-classically correlated pairs of Stokes photons and spin waves. The temporal multiplexed Stokes fields directed into two spatial modes S_R and S_L are collected, respectively. The angles of S_L (S_R) relative to Z axis is 0.14° (−0.14°). The Stokes fields S_R and S_L define the two spin waves *R* and *L*, respectively. The modes S_L and S_R are combined into a spatial *S* at the end of BD2. The field *S* escapes from the cavity coupler (OC). The transmission of OC is 20%. It is coupled into a single-mode fiber and sent to the BSM detection system. Conditioned on a coincident event between D_{S1} or D_{S2} at *i*-th time mode (with $i = 1$ to 12), the two memory ensembles *L* and *R* are projected into an entanglement state. To verify the entanglement state, the *i*-th spin waves in *R* and *L* are converted into the anti-Stokes light fields aS_R and aS_L, respectively, by applying a read pulse. The fields aS_L and aS_R which constrain to the phase-match condition are combined into a spatial mode *aS* after BD1. Escaping from the OC of the cavity, the output field *aS* is sent to the entanglement verification detection system. Panels (b) and (c) are the relevant atomic levels involved in the write and read processes, respectively.

relative to *Z* axis is 0.14° (−0.14°). Along with the generation of the Stokes fields in the channel S_L (S_R) in the *i*-th time mode, a spin wave in *L* (*R*) memory is also created in the *i*-th time bin. The wave vector of the *i*-th spin wave in *L* (*R*) memory is defined by $k^i_{a,L} = k^i_w - k^L_S$ ($k^i_{a,R} = k^i_w - k^R_S$) is the wave vector of atomic spin-wave, k^i_w is the wave vector of the *i*-th write pulse, and k^L_S (k^R_S) is the wave vector of the Stokes photon in mode S_L(S_R), the subscript *a* denote atom.

After the *i*-th write pulse is applied onto the atoms, the joint state of the Stokes field and the associated spin-wave is described as:

$$\left|\psi^i\right\rangle_{L(R)} = \left|0_a\right\rangle\left|0_s\right\rangle + \sqrt{\chi}\left|1^i_a\right\rangle_{L(R)}\left|1^i_s\right\rangle_{L(R)} + O(\chi) \quad (3)$$

where $|0_a\rangle$ ($|0_s\rangle$) denotes the vacuum part, χ is the excitation probability for each time mode alone, with

$\chi^{1-st} = \chi^{2-nd} = \chi^{i-th} = \cdots = \chi^{N-th} = \chi$ assumed, $\left|1_s^i\right\rangle_{L(R)}$ denotes one Stokes photon at the i-th time mode in the S_L (S_R) channel, and $\left|1_a^i\right\rangle_{L(R)}$ the single collective excitation in $L(R)$ spin-wave mode created at the i-th time bin. The single collective spin excitation can be written as

$$\left|1_a^i\right\rangle_{L(R)} = \frac{1}{\sqrt{N_{L(R)}}} \sum_{j=1}^{N_{L(R)}} \exp(-i\vec{x}_{j,L(R)}^i k_{a,L(R)}^i) \left|g_1 \cdots s_j^i \cdots g_{N_{L(R)}}\right\rangle \quad (4)$$

where $N_{L(R)}$ is the number of the atoms for $L(R)$ memory ensemble, $\vec{x}_{j,L(R)}^i$ denotes the spatial position of the j-th atom excited by the i-th write pulse.

In order to generate entanglement between the two memories, we perform single photon interference on Stokes fields S_L and S_R. The temporal multiplexed Stokes fields in the S_L and S_R spatial modes are σ^+ -polarized and transformed into H- and V-polarized by a quarter wave-plate and a half wave-plate, respectively. And then, they are combined into a spatial mode S after BD2. The field S escapes from the cavity coupler (OC) with a transmission of 20%. The output of S field is collected by a single-mode fiber and sent to the measurement system, which includes a half wave-plate HW_S, a polarization beam splitter PBS_S and detectors D_{S1} and D_{S2}. At the two outputs of PBS_S, the field S is changed into two modes $S_+ = \left(S_R + S_L\right)/\sqrt{2}$ and $S_- = \left(S_R - S_L\right)/\sqrt{2}$ when HW_S is set at $\vartheta = 22.5^o$. The fields S_+ and S_- are directed to detectors D_{S1} and D_{S2}, respectively. A click from D_{S1} and D_{S2} in the i-th measurement window heralds that two ensembles are mapped into an entangled state: $\left|\Psi_\pm^i\right\rangle = \left(\left|1_a^i\right\rangle_R|0\rangle_L \pm e^{-i\phi}|0\rangle_R\left|1_a^i\right\rangle_L\right)/\sqrt{2}$, where ϕ is the phase difference between two Stokes fields before they are combined on BD2.

To experimentally verify the entanglement state between the two ensembles, we map the atomic spin-wave into anti-Stokes fields by acting a corresponding σ^+ -polarized read pulse. A feedforward system based on FPGA is utilized to determine the propagation direction of the read pulse. When a Stokes photon is detected in the i-th measurement window, the read pulse with wave-vector $k_R^i = -k_w^i$ is applied on the atoms by a feedforward controlled acousto-optic modulator (AOM). The atomic spin wave $\left|1_a^i\right\rangle_L$ ($\left|1_a^i\right\rangle_R$) is transformed to σ^+ -polarized anti-Stokes field aS_L(aS_R), where its propagation direction is opposite to that of S_L (S_R) field. So, wave vector of anti-Stokes field aS_L(aS_R) is $k_{aS}^L \approx -k_S^L$ ($k_{aS}^R \approx -k_S^R$). The entanglement state between anti-Stokes photons in modes aS_L and aS_R can be written as $\left|\psi_{aS}^\pm\right\rangle = \left(\left|1_{aS}\right\rangle_R|0\rangle_L \pm e^{-i(\phi+\varphi)}|0\rangle_R\left|1_{aS}\right\rangle_L\right)/\sqrt{2}$, where $\left|1_{aS}\right\rangle_{L(R)}$ is the anti-Stokes field with one photon in mode aS_L (aS_R), and φ is the phase difference between two anti-Stokes fields before they are combined on BD1. By controlling the temperature of BD1 and BD2 precisely, the phase difference $\phi + \varphi$ is kept constant. Then, the fields aS_L and aS_R are transformed into H-polarized and V-polarized by wave plates and combined into the field aS on BD1. After the aS field escapes from the cavity, it is collected by a single-mode fiber and sent to the measurement system. The Stokes fields and anti-Stokes fields are resonated with the cavity. The cavity is locked via the Pound-Drever-Hall (PDH) method by using a locking laser pulse, which is coupled to the cavity mode through a beam splitter (BS, R = 95%).

Table 1. The measured P_{mn} at storage time t = 1 μs and t = 150 μs.

Probability	t = 1 μs	t = 150 μs
P_{00}	0.895 ± 0.008	0.937 ± 0.01
P_{01}	0.052 ± 0.003	0.033 ± 0.003
P_{10}	0.053 ± 0.002	0.030 ± 0.003
P_{11}	(5.2 ± 1.2) × 10^{-4}	(4.9 ± 1.6) × 10^{-4}

4. Experimental Results

The entanglement state between two memories can be characterized by measuring the concurrence of entanglement between the fields aS_R and aS_L, which ranges from 0 for a separable state to 1 for a maximally entangled state. The concurrence is measured as $C = \max\left(0, \frac{2|d| - 2\sqrt{P_{00}P_{11}}}{P}\right)$,[49] P_{mn} corresponds to the probability to find m photons in the field aS_R and n photons in the field aS_L in the read process after the Stokes photons are detected, $P = P_{00} + P_{01} + P_{10} + P_{11}$, $d = V\left(P_{10} + P_{01}\right)/2$ is the coherence term between the states $\left|1_{aS}\right\rangle_R|0\rangle_L$ and $|0\rangle_R\left|1_{aS}\right\rangle_L$, V is the visibility of the interference fringes between the anti-Stokes fields aS_R and aS_L when their relative phase θ is scanned.

To measure the interference visibility V, the polarization angle of HW_{aS} is set at $\vartheta = 22.5^o$. The aS field evolves to $aS_+ = \left(aS_R + aS_L\right)/\sqrt{2}$ and $aS_- = \left(aS_R - aS_L\right)/\sqrt{2}$ at the two outputs of PBS_{aS}, which are directed into detectors D_{aS1} and D_{aS2}, respectively. We insert a phase controller before HW_{aS}, which consists of two quarter wave plates and one half wave plate sandwiched in the middle. The relative phase θ between the anti-Stokes fields aS_L and aS_R can be changed by rotating the angle of the half wave plate. Along with the scan of θ, counts in detector D_{aS1} vary as a sinusoidal function, as shown in **Figure 3**. The visibility V can be measured as: $V = \frac{\mathrm{Max}(C_{D_{S1},D_{aS1}}) - \mathrm{Min}(C_{D_{S1},D_{aS1}})}{\mathrm{Max}(C_{D_{S1},D_{aS1}}) + \mathrm{Min}(C_{D_{S1},D_{aS1}})}$, where, $\mathrm{Max}(C_{D_{S1},D_{aS1}})$ ($\mathrm{Min}(C_{D_{S1},D_{aS1}})$) denotes the maximum (minimum) coincidence counts between the Stokes and anti-Stokes fields. Thus, we could get $V = 0.795 \pm 0.015$ at storage time t = 1μs and $V = 0.7 \pm 0.024$ at storage time t = 150 μs. For all experimental results the excitation probability $\chi = 1\%$.

To measure the P_{mn}, we set the polarization angle of HW_{aS} is set at $\vartheta = 0^o$. The probabilities of P_{mn} can be directly measured via photon counting in the fields aS_R and aS_L using detectors D_{aS1} and D_{aS2}, as shown in **Table 1**.

Based on the above measurements, the value of the concurrence of the entanglement between two ensembles can be deduced. The concurrence as a function of the storage time is shown in **Figure 4**. We get a concurrence of C = 0.040(2) at storage time t = 1 μs and C = 0.001(2) at storage time t = 150 μs for $\left|\psi_{aS}^+\right\rangle$. The experimental results show that the entanglement between the two ensembles can be remained for at least 150 μs.

Meanwhile, we measure the intrinsic efficiency of temporal multiplexed quantum memory. The intrinsic efficiency defined by $\eta = \left(P_{01} + P_{10}\right)/\left[\sum_i^{12}\left(P_{D_{S1}}^i + P_{D_{S2}}^i\right)\eta_D\right]$, where, $P_{D_{S1}}^i$ ($P_{D_{S2}}^i$)

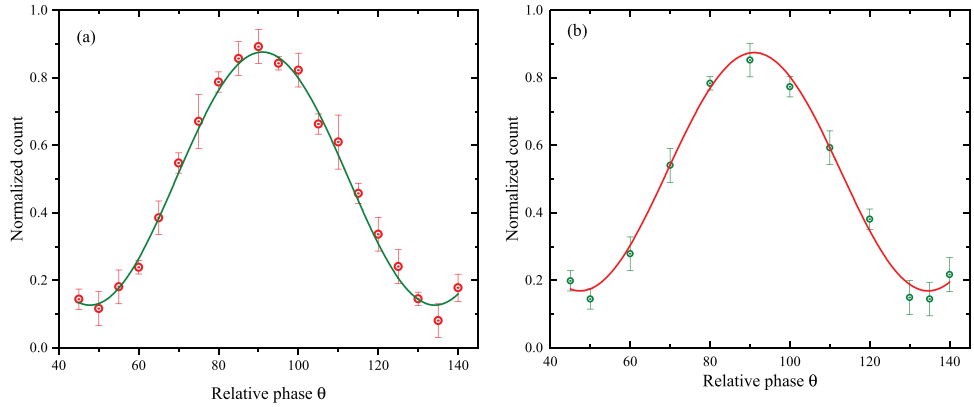

Figure 3. The counts in detector DaS1 as a function of θ for storage time t = 1 μs (a) and storage time t = 150 μs (b).

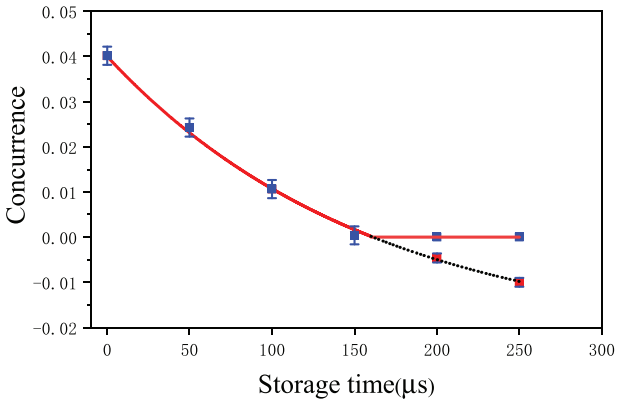

Figure 4. The measured concurrence C as a function of the storage time for $\chi = 1\%$.

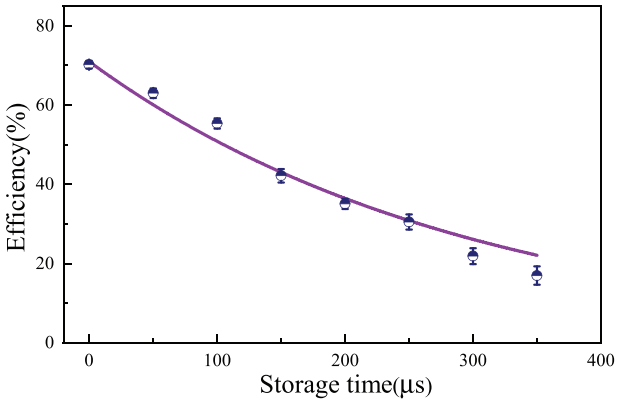

Figure 5. The measured intrinsic efficiency (circles) as a function of storage time.

denotes the probability of detecting Stokes photons at the detectors D_{S1} (D_{S2}) in i-th measurement window, and η_D is the total detection efficiency for anti-Stokes photons. **Figure 5** plots the measured intrinsic efficiency (circles) as a function of storage time. We fit the data according to the function $R(t) = R_0 \exp(-t/\tau_0)$ (shown by the solid curve), which yields the intrinsic efficiency at the zero delay $R_0 = 70.7\%$, together with a memory lifetime $\tau_0 \approx 0.3ms$.

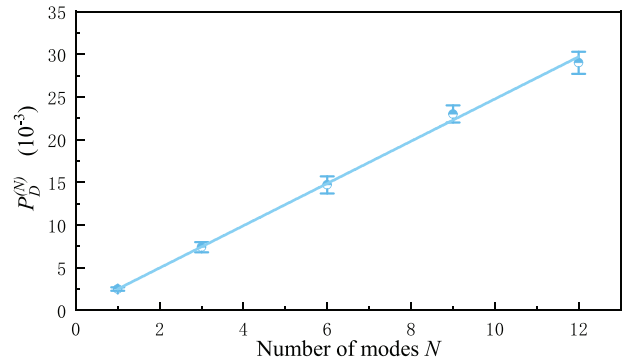

Figure 6. The detection probability of Stokes photon $P_D^{(N)}$ as a function of the number of modes at storage time $t = 1$ μs. The line is the linear fitting according to $P_D^{(N)} = NP_D$, where $P_D = 2.5 \times 10^{-3}$ is the detection probability with single mode.

Then, we present the entanglement generation rate (EGR), as a function of the multiplexed mode number N, shown in **Figure 6**. The EGR with n-mode multiplexing is proportional to the sum of the Stokes photon detection probabilities at the detectors D_{S1} and D_{S2} $P_D^{(N)} = \sum_i^N \left(P^i_{D_{S1}} + P^i_{D_{S2}} \right)$. The result shows the EGR increases linearly with the number of modes, which is good agreement with the theoretical prediction $P_D^{(N)} = NP_D$, where P_D is the EGR for single mode. When the number of modes is 12, $P_D^{(12)}/P_D = 11.79 \pm 0.35$.

Finally, we also measure the concurrence as a function of number of modes at storage time $t = 1$ μs, which is showed in **Figure 7**. As the number of modes increases, the concurrence decreases. We attribute the decrease in concurrence to the crosstalk between the different modes. When one Stokes photon is detected in the i-th measurement window, we retrieve the spin wave by the corresponding read pulse with wave vector k_R^i in the read process. However, the phase-mismatched spin waves generated by all the other write pulses can also be converted the photons. These non-directional photons will direct into the anti-Stokes fields aS_R and aS_L, with a certain probability, which leads to an additional background noise[33] and then cause a decrease in the concurrence. In the future, one can suppress the background noise by using an

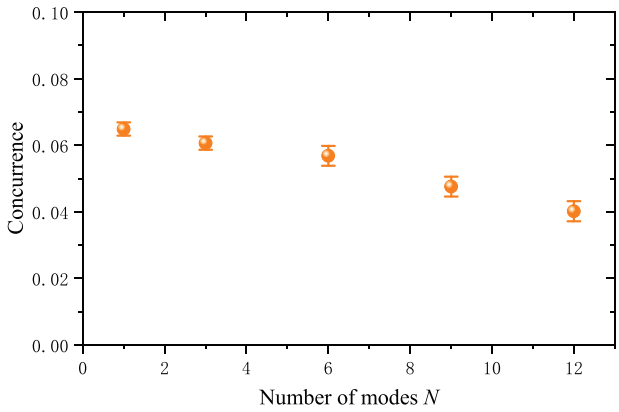

Figure 7. The measured concurrence as a function of mode number at storage time $t = 1$ μs.

asymmetrical photon-collection channel[50] or designing a specially cavity which has different enhancement for the Stokes and anti-Stokes photons.

5. Conclusion and Discussion

We experimentally demonstrate a heralded entanglement distribution between two spin-wave memories via a temporally-multiplexed scheme with a cloud of cold atoms. In the presented experiment, we apply a train of 12 write pulses in time onto the atoms along different directions, which generates multiplexed pairs of Stokes photons and spin waves in time. The temporally multiplexed Stokes photons are collected in two spatial modes S_R and S_L, which define the temporally multimode spin-wave memories R and L, respectively. The spin waves can be effectively transformed into anti-Stokes photons on demand. Compared with the single-mode scheme, the rate of entanglement generation is increased by an order of magnitude (11.8-flod). By using the cavity-enhanced scheme, the on-demand retrieval efficiency of atomic spin waves is up to 70%, which is beneficial for the entanglement swapping between adjacent links. Combining frequency conversion,[48,51–53] our multiplexing quantum repeater link with cavity-enhance holds promise for long-distance communication in optical fiber.

To improve the entanglement distribution rate further, we can load the atoms in optical lattice[11,47] to expand the storage lifetime. In addition, one can realize large-scale multiplexing capability by combining temporal and spatial multiplexing.[54] As shown in Figure 7, the measured concurrence of the two-memory entanglement slowly decreases with the increase in the mode number. The reason for such decrease is due to the additional (background) noise that results from nondirectional emissions from the unwanted spin waves generated in the temporal multimode operation.[33] The degradation of the concurrence is not significant in the current 12-mode storage, but it will become significantly when the number of the temporal modes is further extended in the future. For suppressing the background noise, one can optimize photon-collection channel[50] or use a asymmetric cavity, where, the finesse of the cavity for the Stokes photon is higher than that for the anti-Stokes photon. For the asymmetric cavity scheme, we make a short explanation in the following. It has been pointed out that,[55] by using the asymmetric cavity that resonates with the Stokes field but not with the anti-Stokes field, the additional background noise in the anti-Stokes field is decreased by a factor of $F/1 = F$, where, F is the cavity finesse for the Stokes field, 1 is the cavity finesse for the anti-Stokes field. Recently, H. de Riedmatten's group demonstrated the noise suppression based on this scheme,[31] where, the retrieval efficiency has not been enhanced since the cavity didn't resonate with the anti-Stokes field. It can be expected that the asymmetric cavity with a finesse of F_S for the Stokes field and a finesse of F_{aS} for the anti-Stokes field can suppress the additional noise by a factor of F_S/F_{aS}, where, $F_S > F_{aS}$. In such scheme, F_{aS} can be designed to be ~ 15, which corresponds to the current cavity finesse and then allow one to achieve an enhanced retrieval efficiency same as that in the current work. The price to pay for this scheme is that the finesse of F_S has to be much higher than F_{aS}. The realization of temporal multiplexing quantum repeater link with high retrieval efficiency lays a foundation for the development of practical quantum networks.

Acknowledgements

This work was supported by the National Natural Science Foundation of China (12174235), the Fund for Shanxi Key Subjects Construction (1331), and the Fundamental Research Program of Shanxi Province (202203021221011).

Conflict of Interest

The authors declare no conflict of interest.

Data Availability Statement

The data that support the findings of this study are available from the corresponding author upon reasonable request.

Keywords

heralded entanglement distribution, on-demand retrieval efficiency, spin-wave memory, temporally multiplexed quantum memory

Received: August 28, 2023
Revised: February 27, 2024
Published online: March 18, 2024

[1] H. J. Kimble, *Nature* **2008**, *453*, 1023.
[2] C. Simon, *Nat. Photon.* **2017**, *11*, 678.
[3] S. Wehner, D. Elkouss, R. Hanson, *Science* **2018**, *362*, 303.
[4] S. H. Wei, B. Jing, X. Y. Zhang, J. Y. Liao, C. Z. Yuan, B. Y. Fan, C. Lyu, D. L. Zhou, Y. Wang, G. W. Deng, H. Z. Song, D. Oblak, G. C. Guo, Q. Zhou, *Laser Photonics Rev.* **2022**, *16*, 2100219.
[5] S. L. Severin Daiss, S. Welte, E. Distante, P. Thomas, L. Hartung, O. Morin1, G. Rempe, *Science* **2021**, *371*, 614.
[6] N. Gisin, R. Thew, *Nat. Photon.* **2007**, *1*, 165.
[7] B. Hensen, H. Bernien, A. E. Dreau, A. Reiserer, N. Kalb, M. S. Blok, J. Ruitenberg, R. F. Vermeulen, R. N. Schouten, C. Abellan, W. Amaya, V. Pruneri, M. W. Mitchell, M. Markham, D. J. Twitchen, D. Elkouss, S. Wehner, T. H. Taminiau, R. Hanson, *Nature* **2015**, *526*, 682.
[8] C.-Y. Lu, Y. Cao, C.-Z. Peng, J.-W. Pan, *Rev. Mod. Phys.* **2022**, *94*, 035001.

[9] H. J. Briegel, W. Dür, J. I. Cirac, P. Zoller, *Phys. Rev. Lett.* **1998**, *81*, 5932.
[10] L. M. Duan, M. D. Lukin, J. I. Cirac, P. Zoller, *Nature* **2001**, *414*, 413.
[11] S.-J. Yang, X.-J. Wang, X.-H. Bao, J.-W. Pan, *Nat. Photon.* **2016**, *10*, 381.
[12] B. Zhao, Y. A. Chen, X. H. Bao, T. Strassel, C. S. Chuu, X. M. Jin, J. Schmiedmayer, Z. S. Yuan, S. Chen, J. W. Pan, *Nat. Phys.* **2009**, *5*, 95.
[13] Z. Xu, Y. Wu, L. Tian, L. Chen, Z. Zhang, Z. Yan, S. Li, H. Wang, C. Xie, K. Peng, *Phys. Rev. Lett.* **2013**, *111*, 240503.
[14] Y.-H. Ye, L. Zeng, M.-X. Dong, W.-H. Zhang, E.-Z. Li, D.-C. Li, G.-C. Guo, D.-S. Ding, B.-S. Shi, *Phys. Rev. Lett.* **2022**, *129*, 193601.
[15] M. J. Wang, S. Z. Wang, T. F. Ma, Y. Li, Y. Xie, H. L. Jiao, H. L. Liu, S. J. Li, H. Wang, *Quantum* **2023**, *7*, 903.
[16] X. J. Wang, S. J. Yang, P. F. Sun, B. Jing, J. Li, M. T. Zhou, X. H. Bao, J. W. Pan, *Phys. Rev. Lett.* **2021**, *126*, 090501.
[17] R. Zhao, Y. O. Dudin, S. D. Jenkins, C. J. Campbell, D. N. Matsukevich, T. A. B. Kennedy, A. Kuzmich, *Nat. Phys.* **2009**, *5*, 100.
[18] Y. O. Dudin, A. G. Radnaev, R. Zhao, J. Z. Blumoff, T. A. Kennedy, A. Kuzmich, *Phys. Rev. Lett.* **2010**, *105*, 260502.
[19] Y. Wang, J. Li, S. Zhang, K. Su, Y. Zhou, K. Liao, S. Du, H. Yan, S.-L. Zhu, *Nat. Photon.* **2019**, *13*, 346.
[20] P. Vernaz-Gris, K. Huang, M. Cao, A. S. Sheremet, J. Laurat, *Nat. Commun.* **2018**, *9*, 363.
[21] M. Cao, F. Hoffet, S. Qiu, A. S. Sheremet, J. Laurat, *Optica* **2020**, *7*, 1440.
[22] S. J. Yang, X. J. Wang, J. Li, J. Rui, X. H. Bao, J. W. Pan, *Phys. Rev. Lett.* **2015**, *114*, 210501.
[23] X.-H. Bao, A. Reingruber, P. Dietrich, J. Rui, A. Dück, T. Strassel, L. Li, N.-L. Liu, B. Zhao, J.-W. Pan, *Nat. Phys.* **2012**, *8*, 517.
[24] N. Sangouard, C. Simon, H. de Riedmatten, N. Gisin, *Rev. Mod. Phys.* **2011**, *83*, 33.
[25] C. Simon, H. de Riedmatten, M. Afzelius, N. Sangouard, H. Zbinden, N. Gisin, *Phys. Rev. Lett.* **2007**, *98*, 190503.
[26] Y. F. Pu, N. Jiang, W. Chang, H. X. Yang, C. Li, L. M. Duan, *Nat. Commun.* **2017**, *8*, 15359.
[27] M. Lipka, M. Mazelanik, A. Leszczyński, W. Wasilewski, M. Parniak, *Commun. Phys.* **2021**, *4*, 46.
[28] M. Parniak, M. Dabrowski, M. Mazelanik, A. Leszczyński, M. Lipka, W. Wasilewski, *Nat. Commun.* **2017**, *8*, 2140.
[29] L. Tian, Z. Xu, L. Chen, W. Ge, H. Yuan, Y. Wen, S. Wang, S. Li, H. Wang, *Phys. Rev. Lett.* **2017**, *119*, 130505.
[30] S.-Z. Wang, M.-J. Wang, Y.-F. Wen, Z.-X. Xu, T.-F. Ma, S.-J. Li, H. Wang, *Commun. Phys.* **2021**, *4*, 168.
[31] L. Heller, P. Farrera, G. Heinze, H. de Riedmatten, *Phys. Rev. Lett.* **2020**, *124*, 210504.
[32] P. Farrera, G. Heinze, H. de Riedmatten, *Phys. Rev. Lett.* **2018**, *120*, 100501.
[33] Y. Wen, P. Zhou, Z. Xu, L. Yuan, H. Zhang, S. Wang, L. Tian, S. Li, H. Wang, *Phys. Rev. A* **2019**, *100*, 012342.
[34] H. Liu, M. Wang, H. Jiao, J. Lu, W. Fan, S. Li, H. Wang, *Opt. Express* **2023**, *31*, 7200.
[35] C. Xiong, X. Zhang, Z. Liu, M. J. Collins, A. Mahendra, L. G. Helt, M. J. Steel, D. Y. Choi, C. J. Chae, P. H. Leong, B. J. Eggleton, *Nat. Commun.* **2016**, *7*, 10853.
[36] Z. S. Yuan, Y. A. Chen, B. Zhao, S. Chen, J. Schmiedmayer, J. W. Pan, *Nature* **2008**, *454*, 1098.
[37] T. van Leent, M. Bock, F. Fertig, R. Garthoff, S. Eppelt, Y. Zhou, P. Malik, M. Seubert, T. Bauer, W. Rosenfeld, W. Zhang, C. Becher, H. Weinfurter, *Nature* **2022**, *607*, 69.
[38] V. Krutyanskiy, M. Galli, V. Krcmarsky, S. Baier, D. A. Fioretto, Y. Pu, A. Mazloom, P. Sekatski, M. Canteri, M. Teller, J. Schupp, J. Bate, M. Meraner, N. Sangouard, B. P. Lanyon, T. E. Northup, *Phys. Rev. Lett.* **2023**, *130*, 050803.
[39] Y. Yu, F. Ma, X. Y. Luo, B. Jing, P. F. Sun, R. Z. Fang, C. W. Yang, H. Liu, M. Y. Zheng, X. P. Xie, W. J. Zhang, L. X. You, Z. Wang, T. Y. Chen, Q. Zhang, X. H. Bao, J. W. Pan, *Nature* **2020**, *578*, 240.
[40] D. Lago-Rivera, S. Grandi, J. V. Rakonjac, A. Seri, H. de Riedmatten, *Nature* **2021**, *594*, 37.
[41] H. Li, J. P. Dou, X. L. Pang, T. H. Yang, C. N. Zhang, Y. Chen, J. M. Li, I. A. Walmsley, X. M. Jin, *Optica* **2021**, *8*, 925.
[42] X. Liu, J. Hu, Z. F. Li, X. Li, P. Y. Li, P. J. Liang, Z. Q. Zhou, C. F. Li, G. C. Guo, *Nature* **2021**, *594*, 41.
[43] J. Hofmann, M. Krug, N. Ortegel, L. Gérard, M. Weber, W. Rosenfeld, H. Weinfurter, *Science* **2012**, *337*, 72.
[44] D. L. Moehring, P. Maunz, S. Olmschenk, K. C. Younge, D. N. Matsukevich, L. M. Duan, C. Monroe, *Nature* **2007**, *449*, 68.
[45] S. Chen, Y. A. Chen, B. Zhao, Z. S. Yuan, J. Schmiedmayer, J. W. Pan, *Phys. Rev. Lett.* **2007**, *99*, 180505.
[46] H. Tanji, S. Ghosh, J. Simon, B. Bloom, V. Vuletic, *Phys. Rev. Lett.* **2009**, *103*, 043601.
[47] Y. O. Dudin, L. Li, A. Kuzmich, *Phys. Rev. A* **2013**, *87*, 031801(R).
[48] X. Y. Luo, Y. Yu, J. L. Liu, M. Y. Zheng, C. Y. Wang, B. Wang, J. Li, X. Jiang, X. P. Xie, Q. Zhang, X. H. Bao, J. W. Pan, *Phys. Rev. Lett.* **2022**, *129*, 050503.
[49] J. Laurat, K. S. Choi, H. Deng, C. W. Chou, H. J. Kimble, *Phys. Rev. Lett.* **2007**, *99*, 180504.
[50] Y. Li, Y.-F. Wen, M.-J. Wang, C. Liu, H.-L. Liu, S.-J. Li, Z.-X. Xu, H. Wang, *Phys. Rev. A* **2022**, *106*, 022610.
[51] T. van Leent, M. Bock, R. Garthoff, K. Redeker, W. Zhang, T. Bauer, W. Rosenfeld, C. Becher, H. Weinfurter, *Phys. Rev. Lett.* **2020**, *124*, 010510.
[52] R. Ikuta, T. Kobayashi, T. Kawakami, S. Miki, M. Yabuno, T. Yamashita, H. Terai, M. Koashi, T. Mukai, T. Yamamoto, N. Imoto, *Nat. Commun.* **2018**, *9*, 1997.
[53] B. Albrecht, P. Farrera, X. Fernandez-Gonzalvo, M. Cristiani, H. de Riedmatten, *Nat. Commun.* **2014**, *5*, 3376.
[54] T. S. Yang, Z. Q. Zhou, Y. L. Hua, X. Liu, Z. F. Li, P. Y. Li, Y. Ma, C. Liu, P. J. Liang, X. Li, Y. X. Xiao, J. Hu, C. F. Li, G. C. Guo, *Nat. Commun.* **2018**, *9*, 3407.
[55] C. Simon, H. de Riedmatten, M. Afzelius, *Phys. Rev. A* **2010**, *82*, 010304(R).